SURFACE CHARACTERISTICS OF THREE ACCIDENT TOLERANT FUEL CLADDING MATERIALS AND THEIR POTENTIAL IMPACT ON CRITICAL HEAT FLUX IN LWRS

Rajnikant Umretiya*, Tao Liu*, Zeyun Wu, and Jessika Rojas
Department of Mechanical and Nuclear Engineering, Virginia Commonwealth University
401 West Main Street, Richmond, VA-23284
umretiyarv@vcu.edu, liut8@vcu.edu, zwu@vcu.edu, jvrojas@vcu.edu
*Both authors contributed equally to this work

Donghwi Lee, Tiago A. Moreira, and Mark Anderson
Department of Nuclear Engineering, University of Wisconsin-Madison
1513 University Avenue, Madison, WI-53706
dlee462@wisc.edu, tmoreira@wisc.edu, manderson@engr.wisc.edu

Raul B. Rebak
GE Research
1 Research Circle, Schenectady, NY-12309
rebak@ge.com

ABSTRACT

Accident Tolerant Fuels (ATFs) are novel technologies designed to improve fuel reliability and increase safety margins during design-basis and beyond-design-basis accident scenarios for light water reactors (LWRs). ATF technology can help extend the life of current commercial power reactors. In this study, the surface characteristics of three ATF fuel cladding materials were tested to determine if there was a significant impact on the critical heat flux (CHF) with respect to the current bare zirconium alloy cladding. The ATF claddings included: (1) a Cr-coated Zircaloy-4 produced by physical vapor deposition (coating thickness ~5-6 μm) and cold-spray (coating thickness ~25-30 μm), (2) the FeCrAl alloy APMT (with different surface roughness), (3) the FeCrAl alloy C26M. The baseline reference cladding is the conventional Zircaloy-4. The understanding of ATF materials' surface characteristics and their impact on CHF in flow boiling testing is a critical need as these materials continue to mature for nuclear reactor applications. CHF experiments using these cladding materials were conducted at atmospheric pressure within a flow boiling facility established at the University of Wisconsin. Computational thermal-hydraulic analysis was performed using RELAP5-3D with the above ATF cladding material properties. An input deck and nodalization of the experimental test section was developed to model the experiments. The boundary conditions of the RELAP5-3D model, including the inlet coolant temperature, the outlet pressure, and the mass flow rate, were set to be consistent with those in the experiment. Reasonable model accuracy was received by comparing the RELAP5-3D simulation results against the CHF experimental results.

KEYWORDS

Accident Tolerant Fuel (ATF)
Critical Heat Flux (CHF)
Physical Vapor Deposition (PVD)
Cold Spray
RELAP5-3D

1. INTRODUCTION

The Fukushima Daiichi nuclear power plant accident in 2011 highlighted the weakness of Zircaloy, which is their reactivity with steam, releasing a large amount of hydrogen gas and heat [1]. In this accident, the hydrogen explosions and the release of radionuclides into the environment negatively impacted the public perception of nuclear energy production regarding reliability and safety [1]. However, this accident gave a message to the nuclear community that a decrease in the oxidation rate of Zr-based alloys at high temperatures is a critical factor in improving the fuel assembly's accident tolerance. Thus, accident tolerant fuel (ATF) development is one of the main focus in nuclear materials research nowadays [2]. ATFs are defined as fuels that, in comparison with the standard UO_2– Zircaloy fuel cladding system, can tolerate a loss of active cooling in the reactor core for a considerably longer amount of time, while maintaining or improving the fuel performance during normal operating conditions, design basis accidents, and beyond design basis accidents [3]. In order to qualify for ATF cladding candidate, materials must have several properties such as low oxidation rate, high thermal performance, and stable mechanical properties under normal and accident operational conditions. Among these desired characteristics, improved resistance to high-temperature steam oxidation is considered a priority [4]. Thus, the materials that form protective oxide layers of chromia, alumina, or silica are far more resistant than Zirconium to high-temperature steam oxidation [4]. Many ATF cladding concepts, considered to improve upon the performance of current Zr-based alloys are studied as a group of near-term solutions [5] and long-term technologies [6-7].

The deposition of coatings on the current Zircaloy appears to be one promising near-term ATF cladding concept because the nuclear industry has developed infrastructure, experience, and expertise on Zr-based fuel cladding to the maximum extent possible [8]. This strategy becomes a practical way to improve the existing nuclear fuel system, thus finding intense research interests in two main areas: the coating material and the coating technology. In this regard, different protective coatings and coating methods are being studied. Chromium as a coating material has shown promising results when deposited using the latest generations of PVD and Cold Spray coating techniques [9-11]. For instance, Framatome developed full-length PVD Cr-coated M5® cladding tubes, with $\sim$15 μm thickness of Cr coating [11]. Similarly, Westinghouse is developing Cr-coated cladding of ZIRLO® and optimized ZIRLO™ using a Cold Spray process [12]. Few other coated cladding concepts are under development at Korea Atomic Energy Research Institute [13], Czech Technical University [14], Ukraine [15], Institute for Energy Technology in Norway [16], and other institutes, evidencing enhanced corrosion resistance under normal conditions compared to the classical alloys Zircaloy-2 and Zircaloy-4 [17]. As a nuclear fuel cladding application, especially for coated cladding concept, the coating must adhere to the substrate to avoid spallation [18]. The extraordinary mechanical properties without spallation are reported during ring tensile and ring compression tests for Cr-coated Zircaloy-4 in the literature [19-20]. Studies on coated tube samples have shown good oxidation behavior of Cr-coatings, both in autoclave (415 °C, steam, 100 bars) with conditions close to nominal PWR operating conditions and in high-temperature environments (steam, up to 1300 °C) simulating accidental conditions [10,21]. Studies have also reported good irradiation stability of Cr-coatings [22]. FeCrAl (Iron-chromium-aluminum) alloys are also lead ATF cladding candidates in near-term solutions due to their outstanding high-temperature oxidation resistance [23-25]. The high yield and ultimate tensile strength are reported for unirradiated FeCrAl alloys at different temperatures [26]. On the negative side, FeCrAl alloys have a higher thermal neutron absorption cross-section than Zircaloy. However, this can be compensated by using a thinner cladding with slightly higher enriched fuel to maintain cycle length [24]. Moreover, the fabrication process of FeCrAl alloy is quite similar to current LWR fuel fabrication [27]. Similarly, other long-term cladding technologies include Mo-Zr cladding [28], and SiC_f/SiC cladding [29-30] to provides good corrosion resistance and low thermal neutron absorption cross-section.

Regardless of the favorable characteristics of the cladding materials candidates, understanding their thermal-hydraulic performance is needed and is a current matter of intensive research [31]. Critical heat flux (CHF) is a metric normally used to evaluate the thermal-hydraulic characteristics of these advanced cladding materials. CHF represents the boiling transition point from the nucleate boiling regime with high heat transfer to the low heat transfer film-boiling regime [32-33]. Due to poor heat transfer at CHF, surface temperature abruptly increases, which may cause the cladding failure. Therefore, accurate knowledge and, in general, enhancement of the CHF value is important to designing systems that use nucleate boiling heat transfer. However, due to the complexity and the importance of CHF in the field of boiling heat transfer, numerous empirical correlations have been developed based on corresponding experimental outcomes and theoretical reasoning by previous investigators, with the aims of acquiring knowledge about CHF and eventually enhancing it [34-35]. One of the earlier CHF models, such as Zuber CHF correlation, considered CHF a hydrodynamic instability phenomenon and thus ignored the effects of the boiling surface characteristics [36]. However, the experimental evidence suggests the importance of surface effects on CHF. Key surface parameters that could affect the CHF are surface wettability, surface roughness, liquid-spreading ability, capillarity and wickability, and porosity [37]. Numerous studies have investigated the surface characteristics of ATF candidates that may lead to changes in their thermal-hydraulic performance [38-43]. Thus, the surface characteristics, such as roughness and wettability, of ATF cladding materials must be carefully assessed when evaluating their influence on thermal parameters such as CHF.

The literature has reported a tremendous amount of pool and flow boiling experimental work performed for different ATF materials. However, there is limited work that has been done on the simulation side. The prediction of CHF remains challenging to conceptualize and model because most of the experimental thermal-hydraulic research has focused on obtaining data for specific conditions and geometries. Additionally, the large amount of data that has been collected under corporate supervision remains proprietary. Hence, most CHF predictions rely on comparing tabulated values or applying correlations [32]. However, when compared with experimental data, these correlations have demonstrated limited success due to the complexity of the phenomenon. Furthermore, the effect of many variables such as mass flux, local quality, pressure, flow geometry, axial heat flux profile, wettability, and surface roughness in CHF enhancement is evidenced in the literature [31]. Thus, a single experiment may or may not apply to other situations. The use of data and correlations from uniform heat profile experiments and applying a correction factor to account for the non-uniformity has become standard practice in the nuclear industry, leading to a misunderstanding of the CHF phenomenon. For example, in channels with uniform heat flux, CHF always occurs at the end, where the quality is highest; however, CHF events rarely happen at the exit when non-uniform heat flux profiles are applied. Since most correlations are constructed from the experiments performed using a single heated tube during application in the irregular geometry of the reactor core, these values must then be adjusted for the heated rod bundle geometry. Thus, it is necessary to use simulation tools to understand the thermal-hydraulic response of ATF to design basis accident conditions, such as loos of coolant accident (LOCA).

In this work, the surface characteristics of ATF cladding materials manufactured by commercial industrial techniques were investigated before and after CHF testing. Surface roughness was assessed by contact profilometry as well as atomic force microscopy. The surface wettability of the materials was analyzed by measuring static contact angle using a goniometer. After surface characterization, the samples were tested in an atmospheric pressure flow boiling test facility at the University of Wisconsin. An early thermal-hydraulic evolution was performed by comparing high-resolution experimental data of ATF materials obtained from the flow boiling experiments and results from the computational tool, RELAP5-3D, modeled based on those experiments.

2. EXPERIMENTAL AND COMPUTER MODEL DESCRIPTION

2.1 Materials and Surface Characterization

The cylindrical tube samples used in this study were commercially available nuclear grade Zircaloy-4, FeCrAl alloys (APMT and C26M), Cr-coated Zircaloy-4. Tube segments had an outer diameter of 9.5 mm (wall thickness of 0.51 mm) and 10.26 mm (wall thickness 0.4 mm) for Zr-based alloys and FeCrAl alloys. For coated samples, the Cr coating was deposited on the external surfaces of Zircaloy-4 tubes by using two different techniques, PVD and Cold Spray. Coating parameters for both techniques are provided with details in our previous work [20]. To investigate the effects of surface characteristics on the thermal-hydraulic performance, the samples' surfaces were modified with different roughness (by grinding samples with 600 and 240 grit SiC papers). A Buehler IsoMet low speed-cutting machine with a diamond saw was used to section a slice of the tube specimen for surface characterization. The samples were cleaned in an ultrasonic bath for ~5 minutes and then dried in air. The wettability, quantified by the static contact angle, was measured at ambient conditions using a Rame-hart contact angle goniometer. The experimental setup is reported in our previous study with an inset indicating a DI water droplet deposited on the tube surface looking from a side view during measurements [44]. A 5 μL droplet volume was used for this series of measurements, and the contact angle was recorded within 25s. A total of fifty measurements were collected for all samples following the American Society of Testing Materials (ASTM) standards for contact angle measurements [45]. The surface roughness of the specimens was measured using a stylus profilometer (Mitutoyo Surftest SJ-410; 2 μm tip radius and 60° tip angle). The common surface roughness parameters, Ra, the arithmetic average roughness; Rz, the average of the five highest peaks and the five deepest valleys; and RSm, the arithmetic mean value of the width of profile peaks were measured parallel to the axial direction of the tube following International Organization for Standardization (ISO) standards [46]. All scans, each 5 mm long, were recorded at different locations throughout the tube surface at a traverse speed of 0.5 mm/s. An Atomic Force Microscope (Bruker Dimension Icon) operating in tapping mode was also used to study the surfaces' topographies at the nanoscale. An AFM tip with a radius of curvature less than 10 nm, tip height 10-15 μm, a resonance frequency of 320 kHz, and an approximate force constant of 60 N/m was used to scan the materials' surface. The recorded AFM scans were filtered by a Gaussian mask with a cutoff of 2.5 μm to capture surface features at the nanoscale.

2.2 Flow Boiling CHF Experiments

All materials were tested to measure CHF under atmospheric pressure in a flow boiling facility at the University of Wisconsin-Madison Thermal Hydraulics Lab. The apparatus consists of a closed loop, at which DI-water (resistance higher than 5 MΩ) is drained from the reservoir (opened to the atmosphere) by a centrifugal pump (speed is controlled by a variable frequency drive). Downstream the pump, the water flows through a Coriolis-type mass flow meter and a solenoid valve previously entering the test section. The working fluid is then heated and partially boiled at the test section, passes through a second solenoid valve, and returns to the reservoir, closing the loop. A secondary circuit is used to exchange heat between the water in the loop and a chilled glycol solution, consequently controlling the water temperature. Details about the test facility, e. g. equipment models, range and accuracy, are provided in a previous study [47].

The test section consists of an annular gap, at which the heater (test material) is affixed centered with an outer glass tube. Direct heating by the Joule effect of the cladding rods is used to obtain a uniform heat flux profile. Fig. 1 shows a schematic of the heater. In order to obtain the heat flux applied to the cladding material, electrical losses in the upper and bottom leads (between the voltage sense locations) are estimated and discounted to the total power applied. The accuracy in the estimative of the electrical losses was verified by comparing the total heat absorbed by the water (based on the mass flow rate, and inlet and outlet temperatures) during single-phase flows, and the power applied to the test section discounting electrical losses. As a result, differences smaller than 2% were verified.

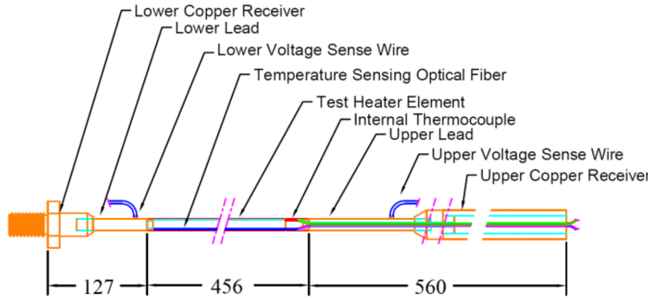

Figure 1. Schematic of the heater assembly (dimensions in mm).

The testing parameters used in this study are listed in Table I. The heat flux was increased by changing the applied voltage with constant inlet conditions (listed in Table I). The heat flux was manually raised from 0 to 2000 kW/m^2 (determined to be below the critical heat flux) by approximately 330 kW/m^2 every 2 minutes. During this manual ramp, process data was recorded at 2 Hz, and the temperature profile was recorded at 5 Hz. When the heat flux value reached 2000 kW/m^2, the heat flux was set to increase automatically every 10 s by 1.25 kW/m^2 until CHF was detected using the LabView process monitoring system (operating at 50 Hz). The detection of CHF was tripped using a rate of 50 Hz by a K-type thermocouple near the outlet, set at 20-25°C above the steady-state temperature of the heater rod. The CHF critical temperature is typically in the range of 190-220 °C. The design of this facility allows automatic power cut off when CHF is detected to stop further heating of the heater rod, which could cause damage to the experimental setup. During CHF event, the LUNA system (distributed fiber temperature measurement) records the temperature of the heater rod for 10 seconds before and after CHF. As a backup CHF trip mechanism, the heater rod resistance deviation was also measured at an acquisition rate of 10 Hz to determine the CHF occurrence. The resistance threshold was purposefully set slightly above the observed operating resistance of the heater rod calculated from the measured voltage drop and applied current to the heater rod. This provided additional safety precautions if the CHF event was initiated far away from the thermocouple's location. The experiments were conducted using water as the working fluid at atmospheric pressure, with 76 °C of subcooling and at a flow rate of 750 kg/m^{2}s. The subcooling condition was selected based on room temperature (24 °C) with atmospheric pressure in order to conservatively simulate the LOCA situation. For the mass flux, although the flow limit of the boiling water reactor is known as 3000 kg/m^{2}s [48], we selected the lower flow rate (750 kg/m^{2}s) to observe the roughness and wettability effect on CHF.

Table I. Testing parameters used for the flow boiling CHF test.

Testing parameter	Value
Cladding tube OD (mm)	9.5 (Zr-based alloys) and 10.26 (FeCrAl alloys)
Cladding wall thickness (mm)	0.51 (Zr-based alloys) and 0.4 (FeCrAl alloys)
Working fluid	Water
Nominal heat flux (MW/m^2)	0 - 3
Inlet temperature (ºC)	24
Inlet pressure (kPa)	115
Nominal mass flux (kg/m^{2}s)	750
Heated length (mm)	457.2
Hydraulic diameter (mm)	10.50 (Zr-based alloys) and 9.74 (FeCrAl alloys)

The uncertainty of measured parameters was considered as the one provided by the manufacturers, and for calculated parameters it was estimated based on the method of sequential perturbation [49]. Details about the uncertainty estimative procedures are provided in previous work [47]. An average uncertainty of 3.24% was found for the heat flux, i.e., CHF.

2.3 Correlations and Relap5-3D Model

2.3.1 Literature on CHF correlations

Several CHF correlations exist in the literature. These correlations are helpful prediction methods for assessing flow systems in LWRs. Some of the most common used CHF correlations are discussed here. The Babcock & Wilcox CHF correlation [50] has been derived based on 601 data points obtained from seven separate tests, including partial and full-length rod bundles with both uniform and non-uniform axial flux shapes. This correlation is only applicable to 17×17 fuel geometry. Another correlation developed from uniformly heated tube experimental data is the Biasi correlation [51]. This correlation does not include any rod bundle geometry or non-uniform power profile modifications, but the nuclear industry uses it as a consistent reference point. To predict CHF in PWRs the Westinghouse Electric Corporation developed the W-3 correlation [52]. Although this correlation has been developed for predicting the DNB (departure from nucleate boiling) using data for an axially uniform heat flux distribution, the correlation incorporates the so-called Tong F-factor to correct non-uniform heat flux distributions. Since this correlation is developed to predict the local DNB heat flux and DNB location, it is limited to high mass flux and low local quality conditions, making it unsuitable for dryout phenomena. Similarly, the EPRI correlation was developed based on rod bundle CHF data, which intrinsically accounts for rod bundle geometry effects. However, the applicable range for this correlation is limited to less than 17 MPa. There are several other correlations in literature developed using pool boiling experimental data that cannot be used for nuclear applications [53-54]. More recently, Groeneveld et. al. [34] gathered worldwide data and organized it into a table format known as look-up table (LUT), which was last updated in 2006. Since the LUT was constructed from many experimental data sets, it remains valid across a wide range of operating conditions with high error in certain regions where a limited number of data samples are used to compose the table. The LUT has multiplicative factors, K-factors, similar to the previously described correlations to account for differences in configuration. Table II summarizes the applicable ranges of pressure, mass flux, and quality for the CHF correlations discussed above.

Table II. Different CHF correlations with their validated ranges.

CHF Correlations	Validated Ranges		
	Mass Flux (kg/m^{2}s)	Pressure (MPa)	Local quality
Babcock & Wilcox	1274 – 5425	12 – 17	-0.03 – 0.22
Biasi	100 – 6000	0.27 – 14.2	0 – 1
W3	1360 – 6780	6.9 – 15.86	-0.15 – 0.15
EPRI	270 – 5560	1.38 – 16.9	-0.25 – 0.75
LUT	0 – 8000	0.1 – 21	-0.5 – 1

2.3.2 RELAP5-3D model description

Computational thermal-hydraulic analysis with the above ATF cladding material properties was performed using RELAP5-3D [55-56], a state-of-the-art system level thermal-hydraulic code developed by the Idaho National Laboratory (INL). An input deck and nodalization of the experimental test section was developed to model the experiment. Fig. 2 shows the nodalization diagram of the RELAP5-3D model for the case study. The tube dimensions listed in Table I were replicated in the model. In RELAP5-3D, the heat transfer packages within the codes always assume fully developed flow, hence only the heated length of the test section was modeled. As shown in Fig. 2, the tube's hydrodynamics component (pipe component) is represented by one flow channel (No.120), which is divided into 50 control volumes along the flow direction. The inlet plenum (flow source) is modeled with a time-dependent control volume (No.100) and the corresponding time-dependent junction. Similarly, the outlet plenum (flow sink) is defined by a single control volume (No.140) and the corresponding single junction.

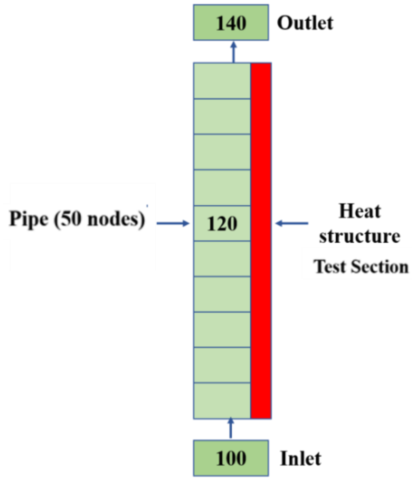

Figure 2. Nodalization diagram of RELAP5-3D model.

In RELAP5-3D, the heat structure (red part) is attached to the coolant (flow channel) and used to define a heat source profile. To show a more detailed temperature distribution in the fuel and cladding, the heat structure is divided into 50 volumes along the axial direction, and 8 mesh intervals along the transverse direction: two mesh intervals on each side of the cladding and six intervals in the middle for the fuel part. Other key physical parameters, including the boundary conditions, pressure, mass flow rate, and temperature of the coolant used in this model are included in Table I, which were consistent with the experiment setup. A minimum timestep of 1×10^{-8} s was used for the dynamic simulations. Due to its general applicability, the Groeneveld look-up table was used to predict CHF in the RELAP5-3D model. To better simulate the flow boiling CHF experiments, the Risk Analysis and Virtual Environment (RAVEN) [56] was coupled with RELAP5-3D. RAVEN is a flexible and multi-purpose data analysis toolset developed by the Idaho National Laboratory (INL) that can be used for sensitivity analysis, uncertainty quantification, regression analysis, probabilistic risk assessment, model optimization, among others. In this study, RAVEN was used to automatically increase the heat flux in RELAP5-3D input files based on the experiment setup, generate multiple RELAP5-3D input files, execute each input file separately, and deliver the output files in sequence.

3. RESULTS AND DISCUSSION

3.1 Surface characterization for ATF materials

Table III provides surface roughness measured by contact profilometry for all samples. Before CHF, the surface roughness parameter Ra for APMT is similar to that of commercial cladding Zircaloy-4 (AR-Zr-4). However, Ra of C26M was twice that of APMT and AR-Zr-4. Similarly, both coated samples evidenced a higher roughness compared to the substrate sample, AR-Zr-4. AFM scans for all samples before CHF testing are provided in Fig. 3. AFM micrographs give a qualitative comparison for all samples, and it helps to understand the surface morphology at the nanoscale. There is a slight increase in the surface roughness recorded for all samples after CHF testing.

Table III. Roughness measurements for all samples before and after CHF testing.

Sample		Contact profilometry measurements (μm)		
		Ra	Rz	RSm
Pre-CHF	APMT	0.40±0.09	3.89±0.99	70.11±7.24
	C26M	0.80±0.12	8.75±1.65	130.27±22.73
	AR-Zr4	0.43±0.06	4.03±0.69	60.94±6.06
	600G-Zr4-Cr-PVD	0.44±0.07	4.37±0.92	65.15±3.67
	AR-Zr4-Cr-CS	1.04±0.07	11.42±1.96	65.09±4.66
Post-CHF	APMT	0.47±0.08	4.68±1.03	76.86±8.22
	C26M	0.90±0.10	9.62±1.83	138.86±22.92
	AR-Zr4	0.54±0.09	-	-
	600G-Zr4-Cr-PVD	0.55±0.08	-	-
	AR-Zr4-Cr-CS	1.11±0.08	-	-

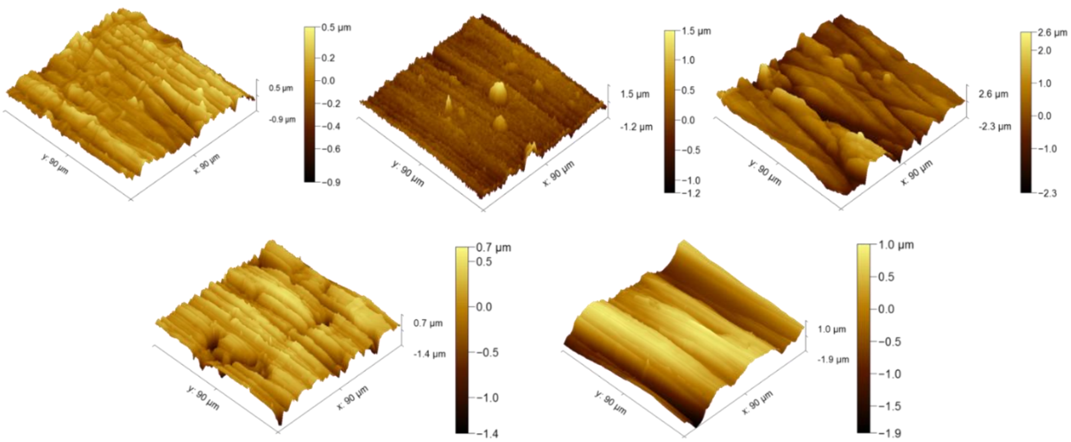

Figure 3. Surface topography of pre-CHF samples by AFM: a) AR-Zr4, b) 600G-Zr4-Cr-PVD, c) AR-Zr4-Cr-CS, d) APMT, and e) C26M.

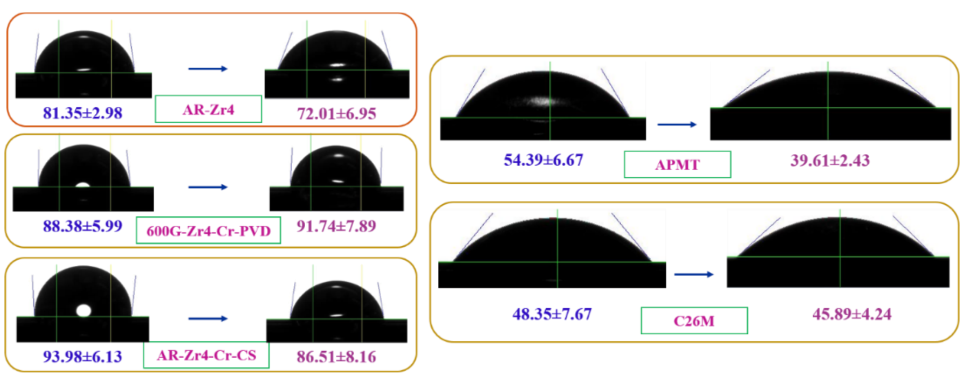

Figure 4. Comparison of static contact angle data pre- and post-CHF samples.

In surface science, the surface wettability is assessed by measuring the contact angle of the water droplet. The contact angle is defined as hydrophilic and hydrophobic when θ is < 90° and θ is > 90°, respectively. Fig. 4 compares the average static contact angle measured at ambient conditions for all samples before and after CHF testing. The surface wettability of post-boiling samples indicated a slight increase in the contact angle of 600-Zr4-Cr-PVD, whereas a noticeable increase in wettability was recorded for both the AR-Zr4 and AR-Zr4-Cr-CS samples. On the other hand, the C26M demonstrated a lower contact angle than the APMT samples before the CHF testing. Our other studies have reported the influence of surface roughness on wetting and spreading behavior for hydrophilic surfaces [20,57]. Furthermore, a lower contact angle was logged for both FeCrAl alloys after CHF testing. The formation of surface oxides during the boiling test is considered the reason for the observed surface roughness and wettability changes. As discussed in reference [58], nanoporous oxide layers are formed during CHF events, which increase wickability and, consequently, wettability.

3.2 Experimental results

The samples AR-Zr4, 600G-Zr4-Cr-PVD, AR-Zr4-Cr-CS, APMT and C26M were used in the CHF experiments. Sample selection for the CHF test, especially for PVD coating, was based on two criteria, surface roughness of 600G-Zr4-Cr-PVD, which is similar to commercial cladding, and improved adhesion strength of the coating compared to AR-Zr4-Cr-PVD. The tests were repeated twice for all samples, and the average CHF values for AR-Zr4, 600G-Zr4-Cr-PVD, AR-Zr4-Cr-CS, APMT and C26M were 2.63 MW/m^2, 2.58 MW/m^2, 2.31 MW/m^2, 2.54 MW/m^2 and 2.26 MW/m^2, respectively. Changes within the uncertainty range of their measurements were noticed for 600G-Zr4-Cr-PVD and the substrate AR-Zr4, while a CHF drop of 12.2% was noticed for AR-Zr4-Cr-CS. The lowest CHF was obtained for C26M (reduction of 14.1%), and a reduction slightly higher than the uncertainty of their measurements was noticed for the APMT (3.4%). It is known from the literature that an increase in surface wettability increases the DNB-type CHF [20,47]. Such behavior is associated with the enhancement of the rewet capability of the surface in case of a dryout event (vapor film formation). Therefore, based on the results shown in Fig. 5(left) (boiling curves obtained based on the thermocouple's data), a reduction in the CHF was expected for 600G-Zr4-Cr-PVD and AR-Zr4-Cr-CS compared to AR-Zr4. Even though showing a higher wettability (i. e., lower contact angle), lower CHF values were observed for the FeCrAl alloy samples (APMT and C26M) compared to Zircaloy-4. As noticed in this figure, under conditions close to the CHF, higher heat transfer coefficients are noticed for AR-Zr4-Cr-CS and FeCrAl alloys. Under low vapor quality and high heat flux conditions, as in the case of the present study, the heat transfer coefficient is dominated by nucleate boiling effects. Therefore, one can indicate from Fig. 5(left) that a higher density of active sites of bubble nucleation is noticed for AR-Zr4-Cr-CS and the FeCrAl alloy samples. This increases the density of bubbles near the heated surface, decreasing, consequently, the DNB-type CHF. It is worth highlighting that even though showing a higher wettability and somewhat a similar roughness (APMT sample) than AR-Zr4, FeCrAl samples provided higher heat transfer coefficients (i. e., higher density of active sites of bubble nucleation). Such behavior is attributed to the fact that the range of cavity sizes within the active range of bubble nucleation depends on the surface scratch diameter (RSm) and not necessarily deepness (Ra and Rz).

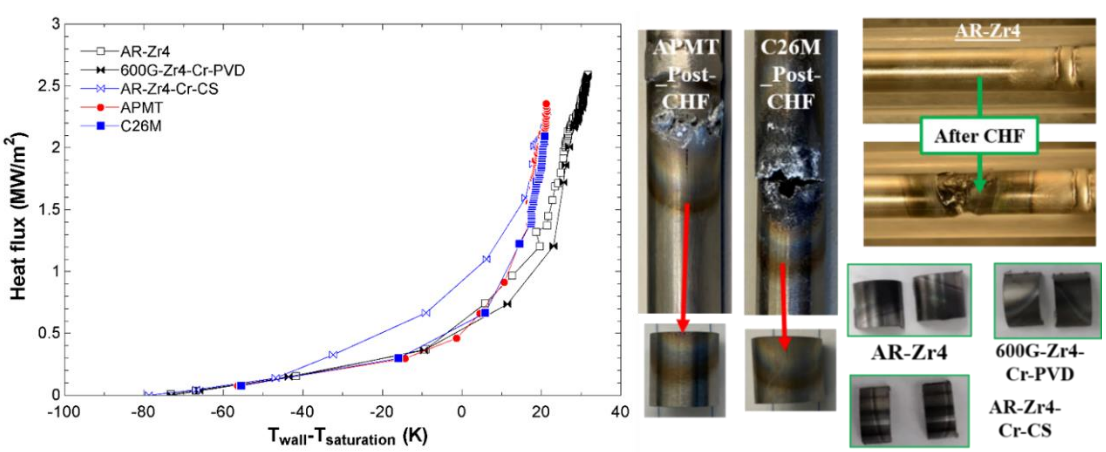

Figure 5. Boiling curves for the tested samples obtained based on the thermocouple's data (left) and post-CHF samples (right).

During the experimental campaign, even with an immediate shut down of the power supply when detecting CHF, cladding temperature rises to sufficiently high temperatures to promote surface oxidation. Tested ATF samples after the CHF experiments are shown in Fig. 5(right).

3.3 Code-to-Experiment comparisons of heat flux and outer surface temperature

Table IV quantifies the percent error of the simulated predictions relative to the experimental values using the CHF and peak cladding temperature (PCT). RELAP5-3D simulation using Groeneveld look-up table, the CHF for all samples was estimated within 10-15% of error. Here, for all samples, simulated CHF was slightly over predicted. This could be because this look-up table method for CHF prediction used in RELAP5-3D does not include surface characteristics. However, an underprediction of the CHF value was noticed for Cr-coated sample (600G-Zr4-Cr-PVD). Better predictions can be made using CHF correlations from literature which incorporates surface characteristics with material properties. On the other hand, simulated PCT values for all samples were low compared to experimental values. This could be because the experimental values are recorded with thermocouples, and when it reaches CHF point, the temperature increases rapidly. In this case, when there is a slight delay in system shutdown, thermocouples give a higher reading. To study the effect of surface characteristics on thermal hydraulic performance, simulated CHF and PCT were acquired for three roughness finish, as-received (0.399 µm), 600-grit polished (0.496 µm) and 240 grit polished (0.776 µm) Zircaloy-4 samples. The simulated values for all surface roughness finishes were almost similar. Here, this surface roughness may not be sufficient to make a significant difference in surface area. In addition, these roughness values were used to calculate friction factor, and they were not used to calculate the CHF directly since look-up table does not take roughness as input. One thing to note here is that the ATF materials own higher wetting characteristics and surface roughness compared to Zircaloy-4, but higher experimental and simulated CHF values were obtained for Zircaloy-4. In the section 3.2, it was also shown that the higher density of active sites of bubble nucleation, noticed by the higher heat transfer coefficient for the FeCrAl alloys compared to Zircaloy-4, has a more significant impact on the CHF than their higher wettability of the surface, resulting in lower CHF values for the FeCrAl alloys.

Table IV. Summary of experimental and simulated CHF and PCT data for all samples.

Material	CHF (MW/m^2)			PCT (°C)		
	Experimental	RELAP5-3D	Error (%)	Experimental	RELAP5-3D	Error (%)
AR-Zr4	2.60	2.72	4.62	175.86	161.05	-8.42
600G-Zr4-Cr-PVD	2.57	2.40	-6.61	179.35	152.85	-14.78
AR-Zr4-Cr-CS	2.28	2.48	8.77	176.25	152.6	-13.42
APMT	2.54	2.56	0.79	212	158.20	-25.38
C26M	2.26	2.56	13.27	212	153.95	-27.38

In the flow boiling CHF experiment, to identify the exact CHF locations, the outer surface temperature profile was measured for all samples using advanced fiber-optic sensors with high temporal/spatial resolution (distance between point to point: 2.5 mm, frequently 100 Hz). CHF was determined as the heat flux where an abrupt temperature increase of 25~30 °C within 1 s compared to the steady-state surface temperature was observed. For example, Fig. 6(a) shows the experimental outer surface temperature profile for the as-received Zircaloy-4 (AR-Zr4), two coated samples (600G-Zr4-Cr-PVD and AR-Zr4-Cr-CS) and both FeCrAl alloys (APMT and C26M). Here, temperature profiles are provided at heat flux equivalent to CHF for all samples. The graph shows that CHF occurred at 80-95% along the heated length, which was expected because the fluid enthalpy (and resultant void fraction) is highest at the top for uniformly heated rods. The void fraction estimation for CHF detection was performed using an in-house MATLAB code after capturing shadowgraph bubble images from the annular channel (data are presented in our previous work [47]). CHF location was also confirmed by visual observation of the discoloration on the surface of all samples following the experiment.

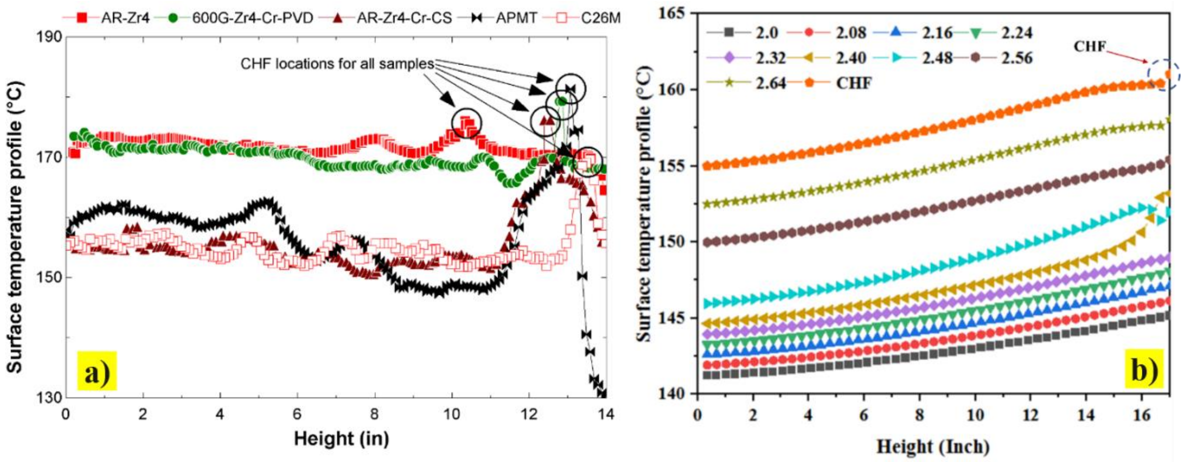

Figure 6. Comparison of experimental tube outer surface temperature for Zircaloy-4, both types of Cr-coatings, and FeCrAl alloys (a); Simulated tube outer surface temperature at different heat flux for Zircaloy-4 (AR-Zr4) sample (b) (all heat flux values are in MW/m^2).

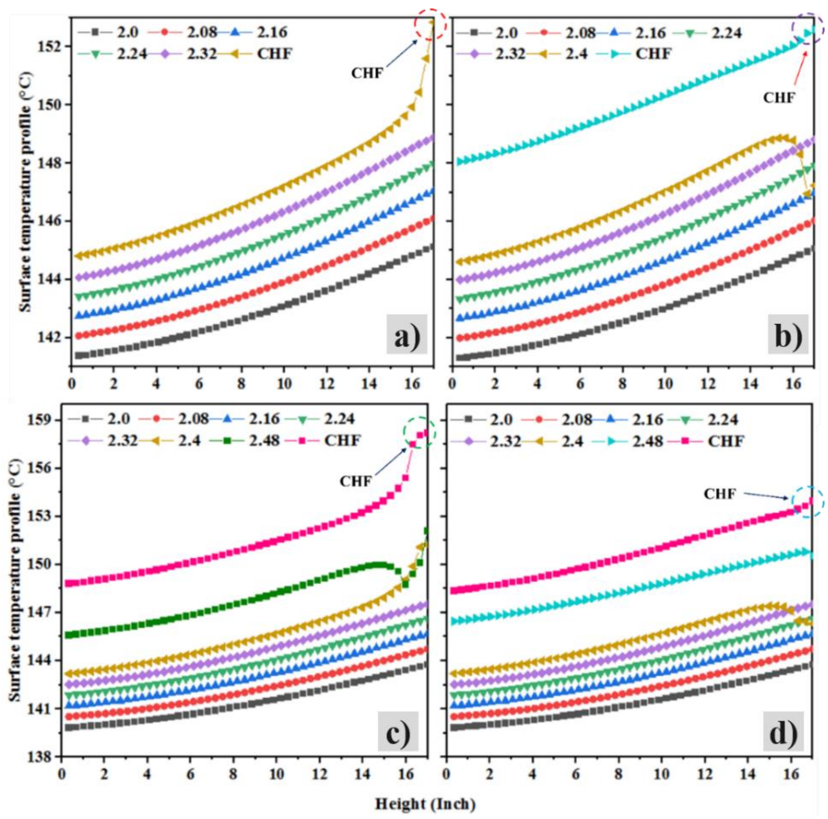

Figure 7. Comparison of simulated tube outer surface temperature at different heat flux for Cr-coated Zircaloy-4: PVD (600G-Zr4-Cr-PVD) (a) and Cold Spray (AR-Zr4-Cr-CS) (b); FeCrAl alloys: APMT (c) and C26M (d) (all heat flux values are in MW/m^2).

On the other hand, RELAP5-3D simulated temperature profiles are shown in Figures 6(b), and 7(a-d) for all materials collected at different heat fluxes, starting from 2 MW/m^2 until it reaches CHF condition. Note that experimental temperature profiles are provided only up to 14-inch length because optical fiber has a termination of 4 inches. Termination is a dead zone for the optical fiber signal; in other words, cordless fiber is required for a good fiber signal to avoid the strong reflection from the fiber end. This data shows how surface temperature increases with heat flux and shows detection of CHF, identified with arrows. At CHF values, in all samples, Zircaloy-4 showed the highest surface temperature throughout the tube, which can also be confirmed from its highest CHF values obtained from experiment and simulation.

4. CONCLUSION

Detailed surface characterization was conducted for ATF cladding candidates, such as APMT, C26M, substrate Zircaloy-4 and Cr-coated Zircaloy-4 produced by two different coating techniques, PVD and Cold Spray. The surface properties of all samples were assessed in terms of roughness and wettability before and after CHF testing. The roughness measured for as-received APMT samples was similar to that of Zircaloy-4, while higher roughness was logged for C26M and coated samples. The contact angles were measured for each surface to evaluate their surface wettability. According to the study for the as-received materials, FeCrAl alloys showed a lower contact angle compared to the substrate Zircaloy-4 and both types of coated samples. Surface characterization of post-CHF samples showed a small increment in surface roughness, while a noticeable increase in the surface wettability was reported for post-CHF samples because of oxide formation on the surface. CHF experiments using these cladding materials were conducted at atmospheric pressure within a flow boiling facility. Experimental results did not show impressive enhancement for ATF materials with wetting friendly and rough surfaces. CHF Computational thermal-hydraulic analysis was then performed using RELAP5-3D with the ATF cladding material properties. The RELAP5-3D simulation results of CHF and PCT were within reasonable error with experimental data.

5. FUTURE WORK

Future work is underway for the development of a transient heat flux model in RELAP5-3D. The model will then be tested for all ATF materials. Furthermore, the effect of surface characteristics such as roughness and wettability in the CHF and HTC will be studied experimentally and verified with existing correlations in the literature. These existing models characterizing the cladding surface effects on CHF may be modified to meet the requirements of ATF candidates. More importantly, sensitivity analysis will be performed to investigate the impact of HTC, and material thermal properties on CHF and PCT. RELAP5-3D heat structure input allows for multipliers on heat transfer coefficients and CHF predicted by their respective correlations. These multiplier values will be chosen in several ways, for instance, the experimental nucleate heat transfer coefficient obtained from the University of Wisconsin was 0.25 times higher for Cr-coated Zircaloy-4 (using Cold Spray) compared to Zircaloy-4; hence, the nucleate boiling heat transfer coefficient multiplier will be varied using RAVEN from 0.1 to 0.5 to determine if this effect could have an impact on CHF. Furthermore, the variation of the thermal properties of ATF, including volumetric heat capacity and thermal conductivity, will be studied within the uncertainty ranges of those properties. The sensitivity of CHF to thermal conductivity and volumetric heat capacity will be calculated. To replicate the enhancement in CHF caused by the transient heating process and to ensure that the experimental CHF was reached, the CHF multiplier will be varied. A large number of combinations will be explored to understand the sensitivities in future work.

ACKNOWLEDGMENTS

This work was supported by the Mechanical and Nuclear Engineering Department at Virginia Commonwealth University (VCU) and The Mechanical Engineering Department University of Wisconsin-Madison with funding from DOE-NEUP (Project number: 17-13-019). The authors wish to thank the staff at the Nanomaterials Core Characterization Facility in the VCU College of Engineering for their technical support with advanced materials characterization.

REFERENCES

[1] The Fukushima Daiichi Accident Report, Non-serial publications, 2015, I.A.E Agency, https://www.iaea.org/publications/10962/the-fukushima-daiichi-accident.

[2] F. Goldner, Overview of the accident-tolerant fuel development, (2013) 14. http://www.iaea.org/inis/collection/NCLCollectionStore/_Public/47/013/47013906.pdf.

[3] S.J. Zinkle, K.A. Terrani, J.C. Gehin, L.J. Ott, L.L. Snead, Accident tolerant fuels for LWRs: A perspective, J. Nucl. Mater. 448 (2014) 374–379. https://doi.org/10.1016/j.jnucmat.2013.12.005.

[4] F. Goldner, Development strategy for advanced LWR fuels with enhanced accident tolerance, Present. to Enhanc. Accid. Toler. LWR Fuels Natl. Metrics Work. Oct. (2012) l5.

[5] H.G. Kim, I.H. Kim, Y.I. Jung, D.J. Park, J.H. Yang, Y.H. Koo, Development of Surface Modified Zr Cladding by Coating Technology for ATF, Top Fuel 2016. (2016) 1157–1163.

[6] K.A. Terrani, S.J. Zinkle, L.L. Snead, Advanced oxidation-resistant iron-based alloys for LWR fuel cladding, J. Nucl. Mater. 448 (2014) 420–435. https://doi.org/10.1016/j.jnucmat.2013.06.041.

[7] K. Lee, D. Kim, Y.S. Yoon, SiC/Si thin film deposited on zircaloy to improved accident tolerant fuel cladding, Thin Solid Films. 660 (2018) 221–230. https://doi.org/10.1016/j.tsf.2018.06.006.

[8] C. Tang, M. Stueber, H.J. Seifert, M. Steinbrueck, Protective coatings on zirconium-based alloys as accident-Tolerant fuel (ATF) claddings, Corros. Rev. 35 (2017) 141–165. https://doi.org/10.1515/corrrev-2017-0010.

[9] H.G. Kim, I.H. Kim, Y. Il Jung, D.J. Park, J.H. Park, B.K. Choi, Y.H. Lee, Out-of-pile performance of surface-modified Zr cladding for accident tolerant fuel in LWRs, J. Nucl. Mater. 510 (2018) 93–99. https://doi.org/10.1016/j.jnucmat.2018.07.061.

[10] M. Shahin, J. Petrik, A. Seshadri, B. Phillips, K. Shirvan, Experimental investigation of cold-spray chromium cladding, Topfuel. (2018) 1–10.

[11] J. Bischoff, C. Delafoy, C. Vauglin, P. Barberis, C. Roubeyrie, D. Perche, D. Duthoo, F. Schuster, J.C. Brachet, E.W. Schweitzer, K. Nimishakavi, AREVA NP's enhanced accident-tolerant fuel developments: Focus on Cr-coated M5 cladding, Nucl. Eng. Technol. 50 (2018) 223–228. https://doi.org/10.1016/j.net.2017.12.004.

[12] E.D. Lahoda, F. Boylan, Overview of Westinghouse Lead Accident Tolerant Fuel Program, (2019) 1–7.

[13] H.G. Kim, J.H. Yang, W.J. Kim, Y.H. Koo, Development Status of Accident-tolerant Fuel for Light Water Reactors in Korea, Nucl. Eng. Technol. 48 (2016) 1–15. https://doi.org/10.1016/j.net.2015.11.011.

[14] J. Krejci, M. Sevecek, Development of Chromium and Chromium Nitride Coated Cladding, Water Reactor Fuel Performance Meeting, (2017).

[15] V.N. Voyevodin, A.S. Kuprin, E.N. Reshetnyak, V.D. Ovcharenko, R.L. Vasilenko, V.V. Bryk, V.A. Belous, P.N. V'yugov, G.N. Tolmachova, Vacuum-arc chromium-based coatings for protection of zirconium alloys from the high-temperature oxidation in air, J. Nucl. Mater. 465 (2015) 400–406. https://doi.org/10.1016/j.jnucmat.2015.06.016.

[16] R. Van Nieuwenhove, V. Andersson, J. Balak, B. Oberländer, In-Pile Testing of CrN, TiAlN, and AlCrN Coatings on Zircaloy Cladding in the Halden Reactor, Zircon. Nucl. Ind. 18th Int. Symp. (2018) 965–982. https://doi.org/10.1520/stp159720160011.

[17] A.T. Motta, A. Couet, R.J. Comstock, Corrosion of Zirconium Alloys Used for Nuclear Fuel Cladding, Annu. Rev. Mater. Res. 45 (2015) 311–343. https://doi.org/10.1146/annurev-matsci-070214-020951.

[18] H.G. Kim, I.H. Kim, Y. Il Jung, D.J. Park, J.Y. Park, Y.H. Koo, Adhesion property and high-temperature oxidation behavior of Cr-coated Zircaloy-4 cladding tube prepared by 3D laser coating, J. Nucl. Mater. 465 (2015) 531–539. https://doi.org/10.1016/j.jnucmat.2015.06.030.

[19] R. V Umretiya, S. Vargas, D. Galeano, R. Mohammadi, C.E. Castano, J. V Rojas, Effect of surface characteristics and environmental aging on wetting of Cr-coated Zircaloy-4 accident tolerant fuel cladding material, J. Nucl. Mater. (2020) 152163.

https://doi.org/https://doi.org/10.1016/j.jnucmat.2020.152163.
[20] R. V. Umretiya, B. Elward, D. Lee, M. Anderson, R.B. Rebak, J. V. Rojas, Mechanical and Chemical Properties of PVD and Cold Spray Cr-coatings on Zircaloy-4, J. Nucl. Mater. 541 (2020) 152420. https://doi.org/10.1016/j.jnucmat.2020.152420.
[21] J.C. Brachet, M. Le Saux, T. Guilbert, M. Tupin, On-going studies at CEA on chromium coated zirconium based nuclear fuel claddings for enhanced Accident Tolerant LWRs Fuel, in: TopFuel 2015, (13-19 Sept. 2015), Zurich, Switzerland.
[22] A. Jain, S. Loganathan, J.D. Kanjilal, G.K. Mehta, High energy heavy ion irradiation of chromium films, Vacuum. 46 (1995) 369–371. https://doi.org/10.1016/0042-207X(94)00081-6.
[23] R.B. Rebak, Alloy Selection for Accident Tolerant Fuel Cladding in Commercial Light Water Reactors, Metall. Mater. Trans. E. 2 (2015) 197–207. https://doi.org/10.1007/s40553-015-0057-6.
[24] R.B. Rebak, Accident Tolerant Materials for Light Water Reactor Fuels, Elsevier, 2020. https://books.google.com/books?id=hSzJDwAAQBAJ.
[25] B.A. Pint, K.A. Terrani, R.B. Rebak, Steam oxidation behavior of fecral cladding, Miner. Met. Mater. Ser. (2019) 1451–1460. https://doi.org/10.1007/978-3-030-04639-2_96.
[26] K.G. Field, M.A. Snead, Y. Yamamoto, and K.A.Terrani, Handbook on the Material properties of FeCrAl alloys for Nuclear Power Production Applications, 2018.
[27] R.B. Rebak, K.A. Terrani, R.M. Fawcett, FeCrAl Alloys for Accident Tolerant Fuel Cladding in Light Water Reactors, (2016) V06BT06A009. https://doi.org/10.1115/PVP2016-63162.
[28] B. Cheng, P. Chou, Y.J. Kim, Evaluations of Mo-alloy for light water reactor fuel cladding to enhance accident tolerance, EPJ Nucl. Sci. Technol. 2 (2016) 5. https://doi.org/10.1051/epjn/e2015-50060-7.
[29] J.D. Stempien, D.M. Carpenter, G. Kohse, M.S. Kazimi, Characteristics of composite silicon carbide fuel cladding after irradiation under simulated PWR conditions, Nucl. Technol. 183 (2013) 13–29. https://doi.org/10.13182/NT12-86.
[30] C.P. Deck, G.M. Jacobsen, J. Sheeder, O. Gutierrez, J. Zhang, J. Stone, H.E. Khalifa, C.A. Back, Characterization of SiC-SiC composites for accident tolerant fuel cladding, J. Nucl. Mater. 466 (2015) 1–15. https://doi.org/10.1016/j.jnucmat.2015.08.020.
[31] Z. Chen, J. Cai, R. Liu, Y. Wang, Preliminary thermal hydraulic analysis of various accident tolerant fuels and claddings for control rod ejection accidents in LWRs, Nucl. Eng. Des. 331 (2018) 282–294. https://doi.org/10.1016/j.nucengdes.2018.03.007.
[32] B. Zohuri, N. Fathi, Thermal-Hydraulic Analysis of Nuclear Reactors, 2015. https://doi.org/10.1007/978-3-319-17434-1.
[33] S. Whitaker, S. Whitaker, 10 – Heat Transfer with Boiling and Condensation, 1977. https://doi.org/10.1016/B978-0-08-017866-0.50016-2.
[34] D.C. Groeneveld, J.Q. Shan, A.Z. Vasić, L.K.H. Leung, A. Durmayaz, J. Yang, S.C. Cheng, A. Tanase, The 2006 CHF look-up table, Nucl. Eng. Des. 237 (2007) 1909–1922. https://doi.org/10.1016/j.nucengdes.2007.02.014.
[35] S. Mori, Y. Utaka, Critical heat flux enhancement by surface modification in a saturated pool boiling: A review, Int. J. Heat Mass Transf. 108 (2017) 2534–2557. https://doi.org/10.1016/j.ijheatmasstransfer.2017.01.090.
[36] N. Zuber, Hydrodynamic Aspects of Boiling Heat Transfer (Thesis), (1959). https://doi.org/10.2172/4175511.
[37] H.F. O'Hanley, Separate Effects of Surface Roughness, Wettability and Porosity on Boiling Heat Transfer and Critical Heat Flux and Optimization of Boiling Surfaces, Am. Inst. Phys. 024102 (2012) 1–161. https://doi.org/10.1063/1.4813450.
[38] A.F. Ali, J.P. Gorton, N.R. Brown, K.A. Terrani, C.B. Jensen, Y. Lee, E.D. Blandford, Surface wettability and pool boiling Critical Heat Flux of Accident Tolerant Fuel cladding-FeCrAl alloys, Nucl. Eng. Des. 338 (2018) 218–231. https://doi.org/10.1016/j.nucengdes.2018.08.024.
[39] S. Xie, M. Shahmohammadi Beni, J. Cai, J. Zhao, Review of critical-heat-flux enhancement methods, Int. J. Heat Mass Transf. 122 (2018) 275–289.

https://doi.org/10.1016/j.ijheatmasstransfer.2018.01.116.
[40] H. Jo, J.M. Kim, H. Yeom, G.C. Lee, H.S. Park, M. Kiyofumi, M.H. Kim, K. Sridharan, M. Corradini, Boiling performance and material robustness of modified surfaces with multi scale structures for fuel cladding development, Nucl. Eng. Des. 291 (2015) 204–211. https://doi.org/10.1016/j.nucengdes.2015.04.032.
[41] H. H. Son, Y. S. Cho, S. J. Kim, Experimental study of saturated pool boiling heat transfer with FeCrAl- and Cr-layered vertical tubes under atmospheric pressure, Int. J. Heat Mass Transf. 128 (2019) 418–430. https://doi.org/10.1016/j.ijheatmasstransfer.2018.09.013.
[42] R.W.L. Fong, T. Nitheanandan, C.D. Bullock, L.F. Slater, and G.A. Mcrae, Effect of Oxidation and Fractal Surface Roughness on the Wettability and Critical Heat Flux of Glass-Peened Zirconium Alloy Tubes, 5th Internal Conference on Boiling Heat Transfer, May 2003, Montego Bay, Jamaica. https://doi.org/10.13140/2.1.1884.8008.
[43] C.S. Sujith Kumar, S. Suresh, C.R. Aneesh, M.C. Santhosh Kumar, A.S. Praveen, K. Raji, Flow boiling heat transfer enhancement on copper surface using Fe doped Al_2O_3-TiO_2 composite coatings, Appl. Surf. Sci. 334 (2015) 102–109. https://doi.org/10.1016/j.apsusc.2014.08.076.
[44] R. Umretiya, D. Ginestro, S. Bilbao y Leon, J. Rojas, B. Elward, M. Anderson, R.B. Rebak, Surface characteristics of accident tolerant fuels cladding and their potential impact in critical heat flux, in: 18th Int. Top. Meet. Nucl. React. Therm. Hydraul. NURETH 2019.
[45] ASTM D7734 (2008), Standard Practice for Surface Wettability of Coatings , Substrates and Pigments by Advancing Contact Angle Measurement[1], https://doi.org/10.1520/D7334-08R13.2.
[46] ISO 4287: 1997(E/F), Geometrical Product Specifications-Surface texture: Profile method-Terms, definations and surface texture parameters.
[47] D. Lee, B. Elward, P. Brooks, R. Umretiya, J. Rojas, M. Bucci, R.B. Rebak, M. Anderson, Enhanced flow boiling heat transfer on chromium coated zircaloy-4 using cold spray technique for Accident Tolerant Fuel (ATF) materials, Appl. Therm. Eng. 185 (2020) 116347. https://doi.org/10.1016/j.applthermaleng.2020.116347.
[48] X. Cheng, U. Müller, Review on Critical Heat Flux in Water Cooled Reactors, Forschungszentrum Karlsruhe, Germany (2003).
[49] B.N. Taylor, C.E. Kuyatt, Guidelines for evaluating and expressing the uncertainty of NIST measurement results, (1994) Technical note 27.
[50] R.H. Wilson, D.A. Farnsworth, R.H. Stoudt, Babcock & Wilcox Correlation of Critical Heat Flux, 1980.
[51] L. Biasi, G.C. Clerici, S. Garriba, R. Sala, A. Tozzi, A New Correlation for Round Duct and Uniform: Heating-Comparison With World Data, 1967.
[52] F.O.R.A.N. Axially, L.S. Tong, W-3 Westinghouse Correlation, J. Nucl. Energy. 21 (1967) 241–248.
[53] G. Liang, I. Mudawar, Pool boiling critical heat flux (CHF) – Part 1, Int. J. Heat Mass Transf. 117 (2018) 1352–1367. https://doi.org/10.1016/j.ijheatmasstransfer.2017.09.134.
[54] G. Liang, I. Mudawar, Pool boiling critical heat flux (CHF) – Part 2: Assessment of models and correlations, Int. J. Heat Mass Transf. 117 (2018) 1368–1383. https://doi.org/10.1016/j.ijheatmasstransfer.2017.09.073.
[55] T.R.-3D© C.D. Team, RELAP5-3D © Code Manual Volume I: Code Structure, System Models and Colution Methods, 2015.
[56] T.R.-3D© C.D. Team, RELAP5-3D © Code Manual Volume II: User’s Guide and Input Requirements, 2015.
[57] R. Umretiya, S. Vargas, R. Uhorchuk, C.E. Castano, J. Rojas, W.M. Street, Aging Effect of Chromium Coated Zircaloy-4 Accident Tolerant Fuel Cladding Material, in: 2019: pp. 744–746.
[58] J. Buongiorno, Can corrosion and CRUD actually improve safety margins in LWRs?, Ann. Nucl. Energy. 63 (2014) 9–21. https://doi.org/10.1016/j.anucene.2013.07.019.